# An Integrated 800-MHz Coupled-Resonator Tunable Bandpass Filter in Silver With a Constant Bandwidth

Mina Rais-Zadeh, *Member, IEEE*, Hossein M. Lavasani, *Student Member, IEEE*,
Aditya Kapoor, and Farrokh Ayazi, *Senior Member, IEEE*

*Abstract*—This paper presents a fully integrated tunable lumped filter on silicon using a low-temperature silver micromachining process. A prototype 836-MHz bandpass filter with a 3-dB bandwidth of 5.9% and insertion loss of 4.8 dB is demonstrated in a second-order coupled-resonator configuration. Continuous tuning of 50 MHz is achieved by electrostatically actuating the lateral air-gap capacitors of the filter. To control the bandwidth while tuning the center frequency, reconfigurable termination impedance is proposed. As a proof of concept, a low-noise amplifier with tunable input impedance is designed to interface with the bandpass filter. The tunable impedance is realized at the input of the low-noise amplifier using a shunt positive metal–oxide–semiconductor transistor. The fabrication, design, and measurement results of the filter are detailed, and future research directions to improve the performance of such filters are discussed.                [2009-0031]

*Index Terms*—Bandpass filters, high-$Q$, lumped filter, micromachining, tunable capacitor, tunable filters.

## I. INTRODUCTION

**M**ICROELECTROMECHANICAL filters offer the advantages of voltage tunability and monolithic integration in a small size. Among the different types of microelectromechanical systems (MEMS) filters, lumped filters that employ tunable or switchable capacitors offer the largest tuning range [1], [2]. Such filters can employ lumped or distributed types of inductors. The physical size of a filter in the very high frequency (VHF) and UHF ranges (30 MHz–3 GHz) becomes large when distributed-type inductors are used. On the other hand, the quality factor ($Q$) of on-chip lumped inductors (e.g., spiral inductors) has not been sufficiently high for applications that require narrow-band filtering with low insertion loss. Consequently, most reconfigurable lumped filters reported in literature to date have either used off-chip inductors or low-loss substrates, such as high-resistivity silicon, flame retardant 4, sapphire, and glass, to achieve low insertion loss [1]–[5]. Due to the challenges involved with the integration of *high-Q* lumped elements in a small form factor on a CMOS-grade silicon substrate ($\rho = 10-20\,\Omega \cdot cm$), narrow-band integrated tunable filters have not been shown in the VHF and UHF ranges.

M. Rais-Zadeh is with the Department of Electrical Engineering and Computer Science, University of Michigan, Ann Arbor, MI 48109-2122 USA (e-mail: minar@umich.edu).

H. M. Lavasani, A. Kapoor, and F. Ayazi are with the School of Electrical and Computer Engineering, Georgia Institute of Technology, Atlanta, GA 30332-0250 USA.

Color versions of one or more of the figures in this paper are available online at http://ieeexplore.ieee.org.
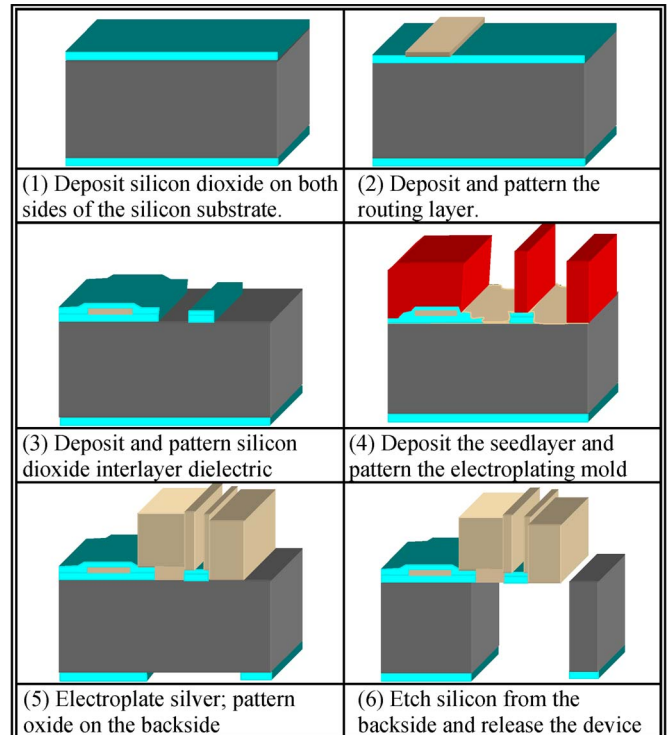
Fig. 1. Fabrication process flow of the tunable filters.

We had previously shown fixed and tunable lumped filters with a 3-dB bandwidth of 9%–30% in the upper UHF range [6], [7]. In this paper, we have investigated the feasibility of implementing a narrow-bandwidth (5.9%) integrated tunable bandpass filter at 800 MHz using a low-temperature post-CMOS-compatible silver micromachining process that is similar to the one introduced in [7]. The results of this research are presented in this paper, demonstrating the first steps toward the implementation of a fully integrated high-performance UHF bandpass filter on a CMOS-grade silicon substrate. In the following sections, we first describe the fabrication process flow of the silver tunable filter. Next, we discuss the electrical and physical design of the filter. We will then present the measured results and discuss ways to improve the performance of the filter.

## II. FABRICATION PROCESS

The low-temperature process used in this paper to implement the filters enables the simultaneous fabrication of high-performance two- and one-port tunable capacitors, as well as high-$Q$ planar inductors. The schematic diagram of the process flow is shown in Fig. 1.
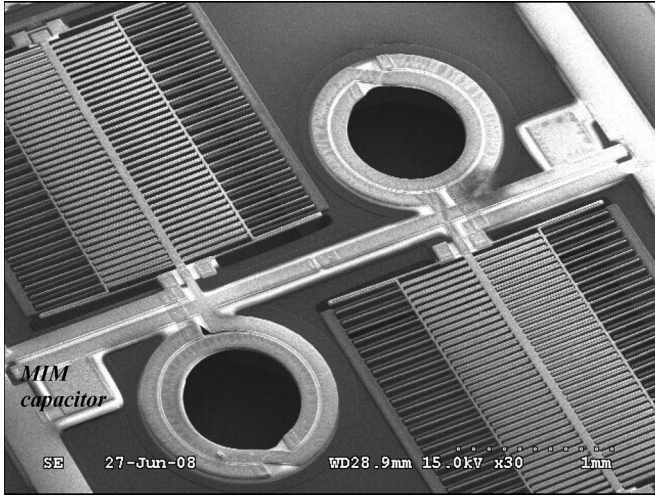
Fig. 2. SEM view of the silver tunable lumped $LC$ coupled-resonator filter.



Fig. 3. Close-up SEM view of the tunable silver capacitor.

First, a 3-$\mu$m-thick plasma-enhanced chemical-vapor-deposited (PECVD) silicon dioxide layer is deposited at 350 °C on the top and the backside of the CMOS-grade silicon substrate. The first metal layer, which consists of 2-$\mu$m gold, is evaporated and patterned. Then, a 1-$\mu$m-thick interlayer PECVD silicon dioxide is deposited. The silicon dioxide layers are then selectively removed from the topside. A seedlayer of titanium–silver–titanium is deposited, and a 20-$\mu$m-thick structural silver is electroplated into a photoresist mold to define the inductors and the tunable capacitors. The mold and the seedlayer are subsequently removed. The silicon dioxide layer deposited on the back is patterned in an inductively coupled plasma system. During this step, the silver features are protected from the fluorine-based plasma by a thin layer of photoresist. Finally, the tunable capacitors are dry-released by selective etching of the silicon substrate from the backside using a deep reactive ion etching system.

An SEM view of the bandpass filter is shown in Fig. 2. The planar spiral inductor is supported by a 4-$\mu$m-thick silicon dioxide membrane while the tunable capacitor is suspended in air. The tunable capacitors are realized using parallel-plate dual-gap configuration, in which the parallel-plate actuator gap is twice the width of the parallel-plate capacitor gap [8]. Air-gap capacitors are used as they benefit from the lowest dielectric loss and exhibit the highest $Q$. If isolated two-port capacitors are desired, the mechanically coupled actuator and capacitor can be electrically isolated using a segment of the silicon dioxide dielectric, as described in [7]. Fig. 3 shows a close-up SEM view of the tunable capacitor.

## III. FILTER DESIGN

### A. Electrical Design

In designing the filter, we targeted a second-order 800-MHz tunable filter with a 3-dB bandwidth of 42 MHz. A two-pole coupled-resonator configuration was used as shown in Fig. 4. This configuration is an alternative realization of a Chebyshev filter, where the series resonator is converted to a parallel resonator using an immittance inverter [9]. A second-order filter
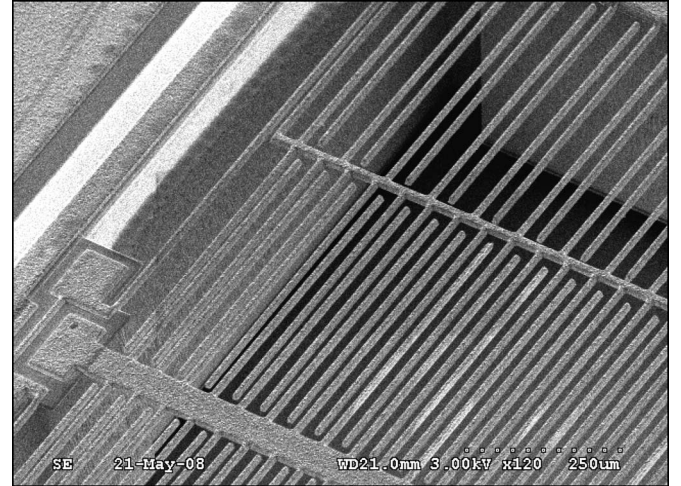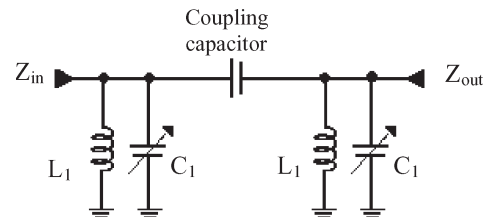


Fig. 4. Schematic of the 800-MHz coupled-resonator tunable bandpass filter.

TABLE I
$q$ AND $k$ VALUES FOR A SECOND-ORDER 0.01-dB CHEBYSHEV CAPACITIVE COUPLED-RESONATOR FILTER

| $n$ | $q_1$ | $q_2$ | $k_{12}$ |
|---|---|---|---|
| 2 | 1.483 | 1.483 | 0.708 |

requires two identical parallel-tuned circuits. Table I presents the $q$ and $k$ parameters for the 0.01-dB ripple Chebyshev capacitive coupled-resonator filter used in this paper [10]. These parameters are used to generate the component values of the filter using the following expressions:

$$Q_{bp} = \frac{f_0}{BW_{3\,\mathrm{dB}}} \qquad (1)$$

$$Q_1 = Q_{bp} \times q_1 \qquad (2)$$

$$Q_2 = Q_{bp} \times q_2 \qquad (3)$$

$$K_{12} = \frac{k_{12}}{Q_{bp}}. \qquad (4)$$

The inductance value can be chosen as desired. Herein, the inductance is chosen to be 4.5 nH, a value that can easily be implemented using surface micromachining techniques. The total nodal capacitance is determined by

$$C_{\mathrm{node}} = \frac{1}{(2\pi f_0)^2 L}. \qquad (5)$$

The coupling capacitors $C_{12}$ are then computed from

$$C_{12} = K_{12} C_{\mathrm{node}}. \qquad (6)$$

TABLE II
COMPONENT VALUES FOR THE SECOND-ORDER
COUPLED-RESONATOR FILTER

| $C_{node}$ | $C_1$ | $C_{12}$ | $L_1$ |
|---|---|---|---|
| 8.8 pF | 8.47 pF | 0.33 pF | 4.5 nH |

The total capacitance connected to each node must be equal to $C_{node}$. Therefore,

$$C_1 = C_{node} - C_{12}. \qquad (7)$$

Table II lists the resulting component values.

Each capacitor in the $LC$ resonator consists of a parallel combination of a fixed metal–insulator–metal capacitor and a lateral tunable capacitor with an initial value of 1.1 pF (Fig. 2). Frequency tuning is achieved by electrostatically varying the tunable capacitors. When tuned, the overall capacitance increases, resulting in a higher resonator $Q$, which, in turn, reduces the 3-dB bandwidth $BW_{3\,dB}$ of the filter. Throughout the literature, to maintain a constant bandwidth across the tuned frequency range, the coupling capacitance is adjusted [11], [12]. In this paper, we study the tuning of the output termination impedance to control the bandwidth. Since, in most applications, the bandpass filter is interfaced with an LNA, we tune the input impedance of the amplifier accordingly. As the input impedance of the LNA drops, the load reflection coefficient $\Gamma_L$ decreases, which, in turn, negatively affects the reflection coefficient at the input terminal of the filter, i.e.,

$$\Gamma_{in} = S_{11} + \frac{S_{12}S_{21}\Gamma_L}{1 - S_{22}\Gamma_L}. \qquad (8)$$

The results are less selectivity for the output tank and a wider bandwidth for the filter. Since the LNA (or any gain block that follows the bandpass filter) has high input impedance, the filter is designed with a high (2000 $\Omega$) output termination to eliminate the need for an extra matching network. The input impedance of the filter is determined to be 200 $\Omega$ using [10]

$$Z_{in}Z_{out} = (2\pi f_0 L Q_1)^2. \qquad (9)$$

If the input termination impedance is maintained constant, from (9), it is evident that, as the output termination impedance $Z_{out}$ decreases, $BW_{3\,dB}$ of the filter increases. The schematic view of the LNA with tunable input impedance is shown in Fig. 5. This design benefits from the high gain and the high stability of the cascaded stage with a noise figure performance that is close to that of a single common-source amplifier. As shown in Fig. 5, the output load of the LNA consists of a lumped $LC$ tank. The resonance frequency of this tank matches the center frequency of the bandpass filter, resulting in a lower overall bandwidth for the cascaded filter and the LNA. With this design, the overall bandwidth of the system is reduced from 42 MHz (the bandwidth of the filter) to 32 MHz, which corresponds to a 24% boost in the $Q$.

*B. EM Simulation*

The Ansoft's high-frequency structural simulator (HFSS) 3-D electromagnetic (EM) full-wave solver [13] was used to optimize the physical design and the layout of the filter. Fig. 6
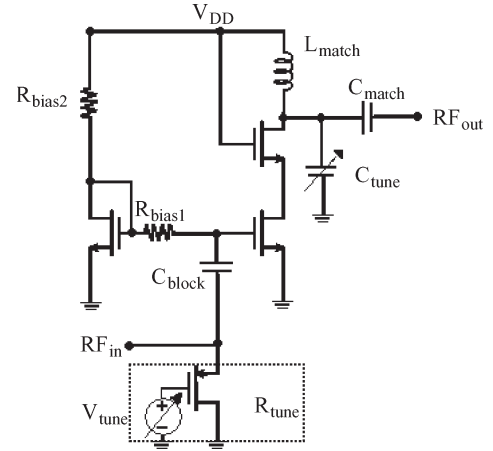


Fig. 5.   Schematic of the LNA with tunable input impedance.
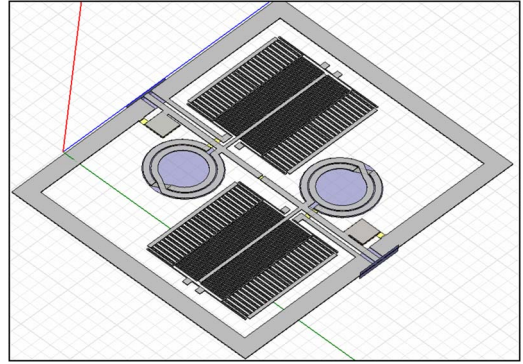


Fig. 6.   HFSS model of the coupled-resonator bandpass filter.

shows the 3-D model of the filter. Symmetrical inductors are employed in the filter as they exhibit higher $Q$ than the conventional spiral-type inductors. The input port of the inductor is connected to the input port of the tunable capacitor using the electroplated silver layer. The ground port of the inductor is connected to the ground port of the tunable capacitor and, accordingly, to the ground box using the routing layer (an underpass). This underpass introduces a small parasitic capacitor that has a negligible effect on the performance of the filter. To reduce the loss, the length of the interconnecting line between the two tanks is minimized by inverting the layout of one tank with respect to the other one. In addition, with this layout, the coupling between the two in-plane inductors is reduced, which results in an improved frequency response.

In the EM simulations, the loss tangent of 0.005 is considered for silicon dioxide, and a conductivity of $6 \times 10^7$ is assumed for the electroplated silver layer. Using these values, the HFSS response of the filter at the initial state is shown in Fig. 7.

The filter shows relatively poor return loss, particularly at the output port, due to the intentional mismatch between the filter and the input and output termination impedances. Due to the same reason, the return loss of the two-pole coupled-resonator filter exhibits only one ripple. However, this mismatch is necessary to interface the filter with the proceeding gain stage without the need for an extra matching network.

Fig. 8 shows a MATLAB simulation, comparing the maximum displacement of the tunable capacitor in the dual-gap
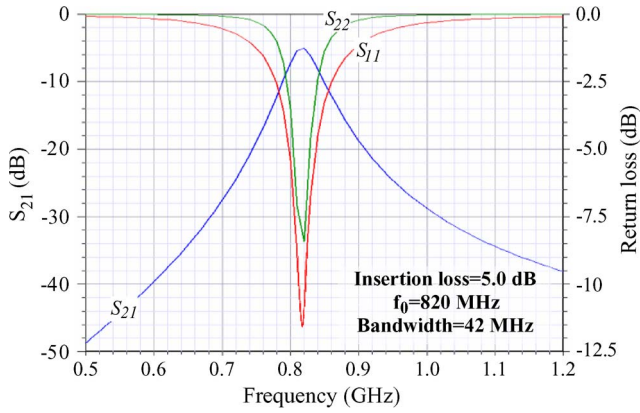
Fig. 7. EM simulated frequency response of the coupled-resonator bandpass filter at the initial state obtained using the HFSS 3-D solver.
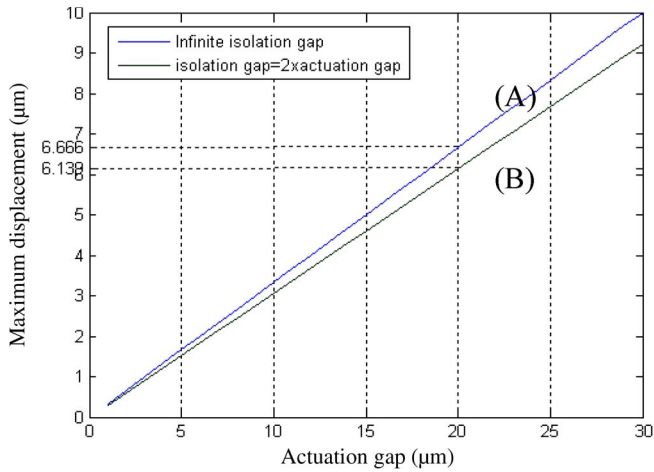


Fig. 8. Simulated maximum displacement of a tunable capacitor in the dual-gap configuration when the isolation gap is set as (A) infinite and (B) twice the actuator gap.

configuration when the isolation gap at the actuator side is set as twice the actuator gap with a case where the isolation gap is infinite. The actuation gap of the tunable capacitor in this paper is 20 $\mu$m, and the isolation gap is 40 $\mu$m. For this configuration, as shown in Fig. 8, the travel range decreases from 6.666 $\mu$m for the infinite isolation case to 6.139 $\mu$m for the 40-$\mu$m isolation, resulting in a drop in the tuning range of the actuators with smaller isolation gaps. Fig. 9 shows the response of the filter when each capacitor is tuned by 6 $\mu$m, showing that a maximum frequency tuning of 85 MHz is possible with this design. At the tuned state, the bandwidth decreases to 35 MHz, and the insertion loss increases by 1 dB.

## IV. RESULTS

The on-wafer $S$-parameter measurements of the fabricated filters and the individual lumped components were carried out using an Agilent E8364B PNA network analyzer and Cascade GSG (I-50) microprobes. DC voltages were applied to the actuators, and the PNA was protected from a possible dc short using bias-tee networks. A calibration is performed using SOLT calibration procedure on Cascade's 50-$\Omega$ standard substrate (101–190). The pad parasitic is not de-embedded from the
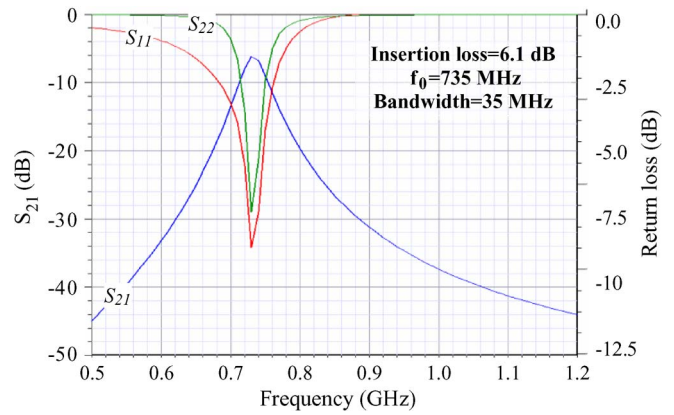


Fig. 9. EM simulated frequency response of the coupled-resonator bandpass filter at the lowest end of the tuning range obtained using the HFSS 3-D solver.
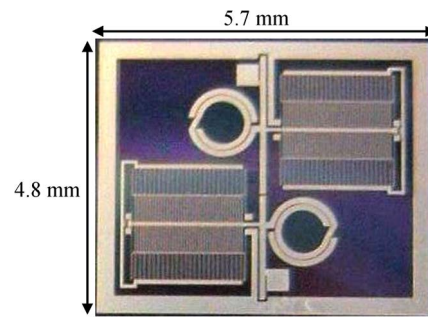


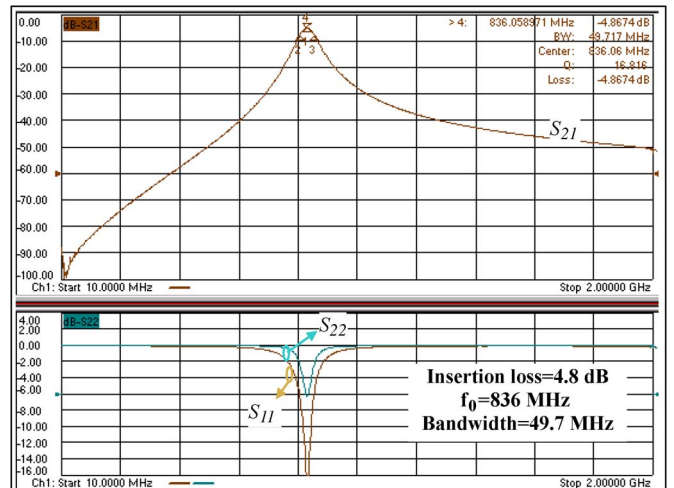Fig. 10. Micrograph of the filter, showing the dimensions of the filter.



Fig. 11. Measured response of the coupled-resonator bandpass filter.

filter frequency response to avoid the underestimation of the filter loss. The filter response with 200-$\Omega$ input and 2000-$\Omega$ output termination impedance is measured by converting the termination impedance of the PNA accordingly.

### A. Tunable Coupled-Resonator Bandpass Filter

Fig. 10 shows the micrograph of the coupled-resonator lumped bandpass filter fabricated on a 10- to 20-$\Omega \cdot$ cm silicon substrate. As shown, this filter occupies 5.7 × 4.8 mm$^2$ of the die area, which is considered small compared with other reported tunable lumped filters operating in this frequency range
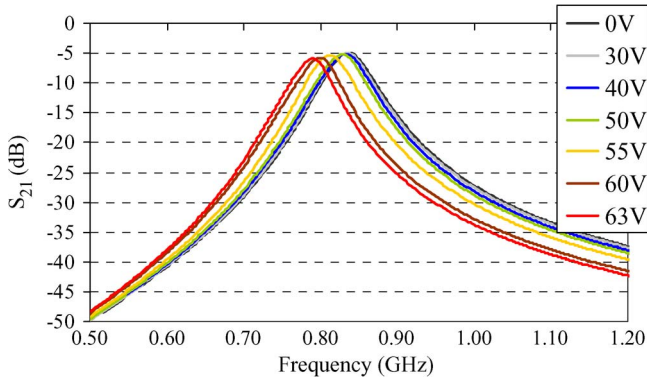
Fig. 12.   Measured electrostatic tuning of the filter, showing a tuning range of 50 MHz. (Inset) Equal dc voltage applied to the tunable capacitors.
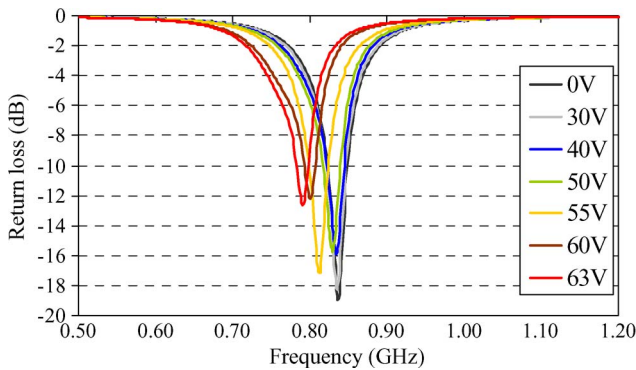


Fig. 13.   Measured return loss of the filter at the input port across the tuning range. (Inset) Equal dc voltage applied to the tunable capacitors.

[14], [15]. Fig. 11 shows the measured $S$-parameter of the band-pass filter. The filter exhibits a 3-dB bandwidth of 49 MHz at 836 MHz, with insertion loss of 4.8 dB. As shown in Fig. 11, the filter response is spurious-free in a broad range of frequency (10 MHz–2 GHz). The HFSS response is in good agreement with the measured response (compare Figs. 7 and 11). The slight discrepancy in the center frequency and the bandwidth is attributed to the imprecise thickness of the electroplated silver layer. In addition, due to the residual stress in the silver electroplated film, the tunable capacitor fingers are slightly curled out of the plane of the substrate. The curled fingers do not overlap as much as expected, resulting in higher $f_0$ and bandwidth for the fabricated filter.

Figs. 12 and 13 show the measured electrostatic tuning characteristic of the coupled-resonator filter when equal dc voltages are applied to the tunable capacitors. As expected, the bandwidth of the filter reduces from 49.7 to 43.7 MHz when tuning the center frequency of the filter from 836 to 786 MHz. To maintain a constant bandwidth, the output termination of the filter is adjusted as discussed in the next section.

### B. System-Level Results

The proposed LNA is interfaced with the measured $S$-parameters of the fabricated filter, imported into Advance Design System (ADS) as a data item. The combined coupled-resonator filter and the LNA show greater than 10 dB of gain across the passband (Fig. 14). The LNA is designed in a 1P6M
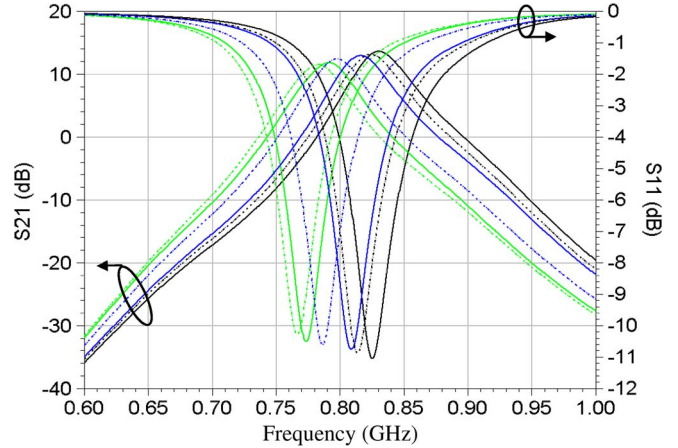


Fig. 14.   Simulated frequency response of the cascaded filter and the tunable-input LNA. The bandwidth of the filter is 35 MHz across the tuning range.

0.18-$\mu$m CMOS process and consumes 2.7 mA out of a 1.8-V supply. The 3-dB bandwidth of the cascaded filter and the LNA is lesser than that of the individual bandpass filter. At the initial state of the capacitors, the overall bandwidth is 35 MHz. As the filter is tuned, if no adjustment is made to the input of the LNA, the overall bandwidth drops to 31 MHz. Tunable impedance is realized at the input of the LNA using a shunt tunable positive metal–oxide–semiconductor (PMOS) transistor to keep the bandwidth constant. The PMOS transistor is operated in the linear region. To tune the impedance, $V_{GS}$ of the transistor is changed from 1.6 to 0.9 V. Since the value of this resistor is large, its associated noise is small and, therefore, has a minimal effect on the overall noise figure of the LNA. Tuning this impedance from 2000 to 800 $\Omega$ increases the bandwidth of the filter at the tuned state from 31 to 35 MHz, resulting in a constant bandwidth of 35 MHz across the entire tuning range (Fig. 14).

### V. DISCUSSION

The tuning range and the insertion loss of the filter can be further improved. To shed light on the true limits of the technology, some approaches to improve the performance of the filter are described in this section and discussed in detail.

### A. Tuning Range

The fixed capacitors form a large fraction of the total capacitance in each $LC$ resonator and, hence, heavily load the overall capacitance tuning range. Consequently, whereas the application of 63 V results in more than 2$\times$ capacitance change for the tunable capacitors (Fig. 15), the overall capacitance change is no more than 12%. The tuning of the coupled-resonator filter can significantly be improved by increasing the ratio of the tunable-to-fixed capacitor. To increase the overall tuning of the capacitance, one can reduce the parallel-plate gap spacing or place several identical tunable capacitors in parallel at the cost of increased area and parasitics. In addition, as discussed in Section IV, the tunable capacitor fingers are slightly curled out of the plane of the substrate due to the residual stress in
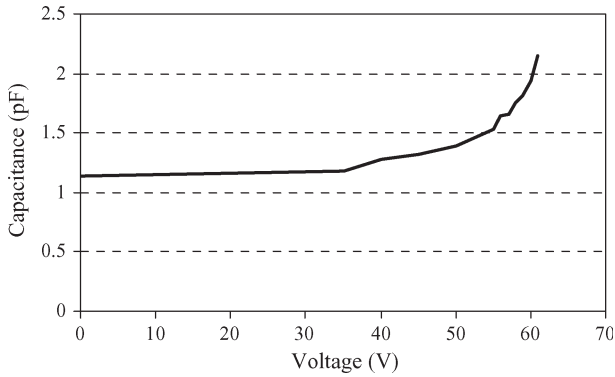
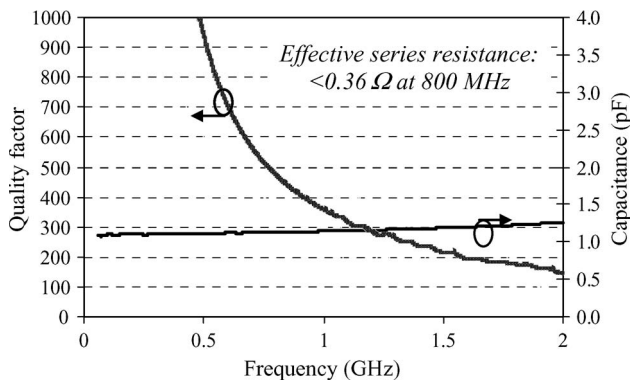Fig. 15. *C–V* tuning curve of the tunable capacitor.



Fig. 16. Measured embedded characteristic of the tunable silver capacitor. The trade line of the measured data is shown for the quality factor.
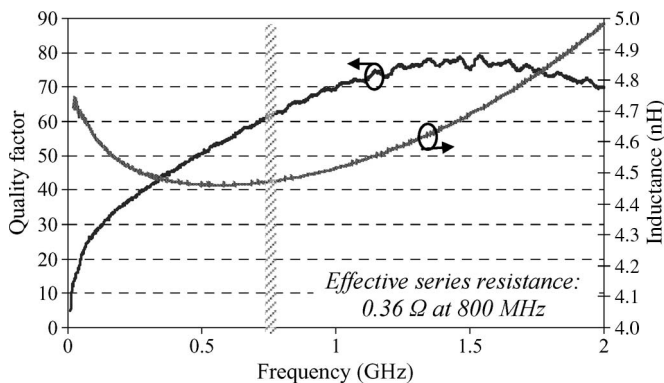


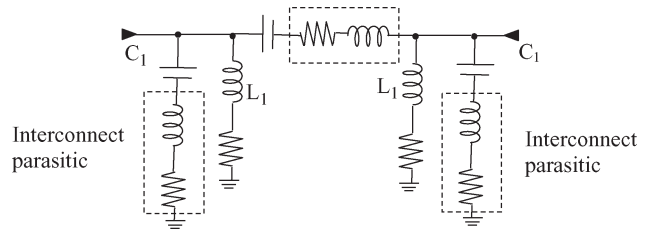Fig. 17. Measured embedded characteristic of the on-chip silver inductors.



Fig. 18. Equivalent electrical model of the bandpass filter using the measured characteristic of the individual lumped components.
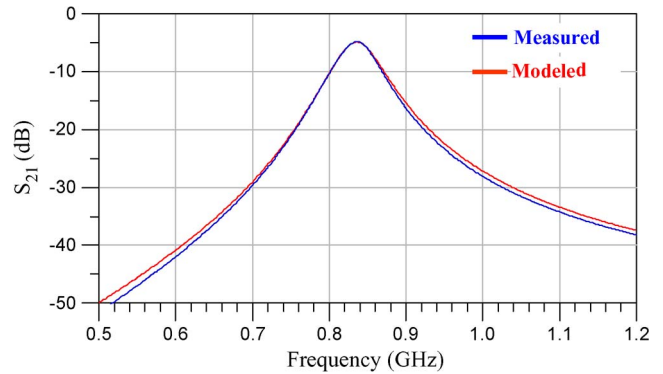


Fig. 19. Comparison of the measured and modeled insertion losses of the coupled-resonator filter.
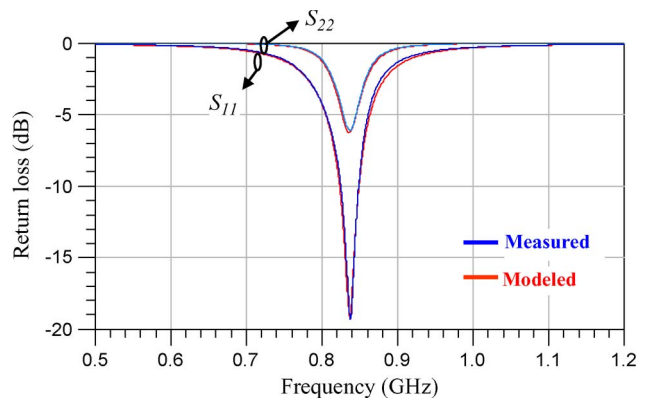


Fig. 20. Comparison of the measured and modeled return losses of the coupled-resonator filter.

the silver layer. This results in a smaller tunable capacitance density, further reducing the tuning range.

### B. Individual Q

The quality factor of the individual components was measured, and the filter was subsequently modeled using the measured data. Fig. 16 shows the measured characteristic of a stand-alone tunable silver capacitor that is identical to the one used in the filter (fabricated on the same substrate). As shown, this capacitor has a very high $Q$ at the center frequency of the filter, owing to the excessive reduction of both the metal loss and the substrate loss. The measured characteristic of the on-chip inductors is shown in Fig. 17. Although a high $Q$ of 79 is

achieved for the integrated inductor at 1.54 GHz, the inductor $Q$ at the filter passband (the hatched area) is not at its highest possible value.

Using the measured characteristics of the individual components, the electrical model of the filter is derived (Fig. 18). The long lines interconnecting the two resonators, as well as the lines connecting the tunable capacitors to the ground plane, are modeled as inductors in series with small resistors. The values of these parasitic inductors and resistors are adjusted such that the modeled response fits that of the measurement. Figs. 19 and 20 compare the measured and modeled frequency responses of the filter, showing an excellent agreement. From the fitted model, $Q$ of each parallel $LC$ tank is extracted to be 50. This is in full agreement with the $Q$ of the tank computed from the

measured $Q$ of the individual components, as shown in Figs. 16 and 17, and using

$$\frac{1}{Q_{\text{tank}}} = \frac{1}{Q_{\text{inductor}}} + \frac{1}{Q_{\text{capacitor}}}. \quad (10)$$

## VI. Conclusion and Future Work

The design, fabrication, and characterization of a micromachined second-order coupled-resonator filter have been presented. The filter has been implemented using a post-CMOS-compatible fabrication process that offers the simultaneous implementation of high-quality-factor on-chip inductors and tunable capacitor. An LNA with tunable input impedance has been designed and interfaced with the measured $S$-parameter of the filter to maintain a constant bandwidth across the tuned frequency range. The cascaded filter and the LNA exhibited a constant bandwidth of 35 MHz and have been tuned from 836 down to 786 MHz.

In the prototype demonstration, the tunable capacitors formed a small fraction of the total capacitance of each resonator. Therefore, the tuning range of the coupled-resonator filter was limited. The tuning can significantly be improved by increasing the ratio of the tunable-to-fixed capacitance. The insertion loss can be improved by increasing the thickness of the metal layers and improving the quality (loss tangent) of the interlayer dielectric. Nonetheless, this proof-of-concept demonstration shows a great promise for the monolithic integration of MEMS tunable filters and CMOS circuits.

## Acknowledgment

## References

[1] R. M. Young, J. D. Adam, C. R. Vale, T. T. Braggins, S. V. Krishnaswamy, C. E. Milton, D. W. Bever, L. G. Chorosinski, L. Chen, D. E. Crockett, C. B. Freidhoff, S. H. Talisa, E. Capelle, R. Tranchini, J. R. Fende, J. M. Lorthioir, and A. R. Torres, "Low-loss bandpass RF filter using MEMS capacitance switches to achieve a one-octave tuning range and independently variable bandwidth," in *Proc. IEEE IMS*, Philadelphia, PA, Jun. 2003, pp. 1781–1784.
[2] J. Nath, D. Ghosh, J.-P. Maria, A. I. Kingon, W. Fathelbab, P. D. Franzon, and M. B. Steer, "An electronically tunable microstrip bandpass filter using thin-film barium–strontium–titanate (BST) varactors," *IEEE Trans. Microw. Theory Tech.*, vol. 53, no. 9, pp. 2707–2712, Sep. 2005.
[3] K. Entesari, K. Obeidat, A. R. Brown, and G. M. Rebeiz, "A 25–75-MHz RF MEMS tunable filter," *IEEE Trans. Microw. Theory Tech.*, vol. 55, no. 11, pp. 2399–2405, Nov. 2007.
[4] C. A. Hall, R. C. Luetzelschwab, R. D. Streeter, and J. H. Vanpatten, "A 25 Watt RF MEM-tuned VHF bandpass filter," in *IEEE MTT-S Int. Microw. Symp. Dig.*, Jun. 2003, pp. 503–506.
[5] L. A. Borwick, P. A. Stupar, J. F. DeNatale, R. Anderson, and R. Erlandson, "Variable MEMS capacitors implemented into RF filter systems," *IEEE Trans. Microw. Theory Tech.*, vol. 51, no. 1, pp. 315–319, Jan. 2003.
[6] M. Rais-Zadeh, P. A. Kohl, and F. Ayazi, "High-$Q$ micromachined silver passives and filters," in *IEDM Tech. Dig.*, San Francisco, CA, Dec. 2006, pp. 727–730.

[7] M. Rais-Zadeh and F. Ayazi, "Small-bandwidth integrated tunable bandpass filters for GSM applications," in *Proc. IEEE Int. Conf. MEMS*, Tucson, AZ, Jan. 2008, pp. 1032–1035.
[8] M. Rais-Zadeh and F. Ayazi, "High-Q tunable silver capacitors for RFIC's," in *Proc. IEEE Meeting Silicon Monolithic Integr. Circuits RF Syst. (SiRF)*, Long Beach, CA, Jan. 2007, pp. 169–172.
[9] T. H. Lee, *Planar Microwave Engineering*. Cambridge, U.K.: Cambridge Univ. Press, 2004.
[10] A. B. Williams and F. J. Taylor, *Electronic Filter Design Handbook*, 2nd ed. New York: McGraw-Hill, 1988.
[11] S. J. Park and G. M. Rebeiz, "Low-loss two-pole tunable filters with three different predefined bandwidth characteristics," *IEEE Trans. Microw. Theory Tech.*, vol. 56, no. 5, pp. 1137–1148, May 2008.
[12] C. Palego, A. Pothier, A. Crunteanu, M. Chatras, P. Blondy, C. Champeaux, P. Tristant, and A. Catherinot, "A two-pole lumped-element programmable filter with MEMS pseudodigital capacitor banks," *IEEE Trans. Microw. Theory Tech.*, vol. 56, no. 3, pp. 729–735, Mar. 2008.
[13] [Online]. Available: www.Ansoft.com/HFSS
[14] M. K. Roy and J. Richter, "Tunable ferroelectric filters for software defined tactical radios," in *Proc. 15th IEEE ISAF*, Sunset Beach, NC, Jul. 2006, pp. 348–351.
[15] A. Tombak, J. P. Maria, F. T. Ayguavives, J. Zhang, G. T. Stauf, A. I. Kingon, and A. Mortazawi, "Voltage-controlled RF filters employing thin-film barium–strontium–titanate tunable capacitors," *IEEE Trans. Microw. Theory Tech.*, vol. 51, no. 2, pt. 1, pp. 462–467, Feb. 2003.

**Mina Rais-Zadeh** (S'03–M'08) received the B.S. degree in electrical engineering from Sharif University of Technology, Tehran, Iran, and the M.S. and Ph.D. degrees in electrical and computer engineering from Georgia Institute of Technology, Atlanta, in 2005 and 2008, respectively.

From August 2008 to 2009, she was a Postdoctoral Research Fellow with the Integrated Microelectromechanical Systems (MEMS) Group, Georgia Institute of Technology. Since January 2009, she has been with the University of Michigan, Ann Arbor, where she is currently an Assistant Professor in the Department of Electrical Engineering and Computer Science. Her research interests include passive micromachined devices for communication applications, CMOS-MEMS integration, and microfabrication process development.

**Hossein M. Lavasani** (S'99) was born in Tehran, Iran, in 1979. He received the B.S. degree in electrical engineering from Sharif University of Technology, Tehran, in 2001, and the M.S. degree from Arizona State University, Tempe, in 2003. He is currently working toward the Ph.D. degree at Georgia Institute of Technology, Atlanta.

From 2003 to 2004, he was with the Medtronics Microelectronics Center, Phoenix, AZ, as an IC Design Engineer, where he was in charge of developing logic and mixed-signal circuits for microcontroller units used in pacemakers. His research interests include the area of interface circuit design and characterization for high-frequency MEMS-enabled radio transceivers, as well as microwave filter design.

**Aditya Kapoor** was born in Mumbai, India, in 1982. He received the B.E. degree in electronics and communications from Maharshi Dayanand University, Rohtak, India, in 2004, and the M.S. degree from Michigan Technological University, Houghton, in 2006, under the guidance of Dr. Paul Bergstrom, working toward the characterization and optimization of FIB patterned tunneling barriers for use in single-electron transistors.

As an undergraduate student, he worked on three summer internships with the Ministry of Defense, Government of India. Since September 2006, he has been with the Integrated Microelectromechanical Systems (MEMS) Group, School of Electrical and Computer Engineering, Georgia Institute of Technology, Atlanta. His research interests include the areas of RF MEMS, microfabrication and nanofabrication technologies, and integrated microsystems.

**Farrokh Ayazi** (S'96–M'00–SM'05) received the B.S. degree in electrical engineering from the University of Tehran, Tehran, Iran, in 1994, and the M.S. and Ph.D. degrees in electrical engineering from the University of Michigan, Ann Arbor, in 1997 and 2000, respectively.

Since December 1999, he has been with the Georgia Institute of Technology, Atlanta, where he is currently an Associate Professor in the School of Electrical and Computer Engineering. His research interests include the areas of integrated microelectromechanical and nanoelectromechanical resonators, IC design for MEMS and sensors, RF MEMS, inertial sensors, and microfabrication techniques.

Prof. Ayazi is an Editor for the JOURNAL OF MICROELECTROMECHANICAL SYSTEMS and serves on the Technical Program Committees of the IEEE International Solid State Circuits Conference and the International Conference on Solid State Sensors, Actuators and Microsystems (Transducers). He was a recipient of the 2004 National Science Foundation CAREER Award, the 2004 Richard M. Bass Outstanding Teacher Award, and the 2001 and 2002 Georgia Institute of Technology College of Engineering Cutting Edge Research Award. He was also a recipient of a Rackham Predoctoral Fellowship from the University of Michigan for 1998 and 1999.